CHAPTER IV
CONVERSION OF GLYCEROL TO AROMATIC HYDROCARBONS OVER Zn–PROMOTED HZSM–5
(Published in Catalysis Today)

4.1 Abstract

Catalytic conversion of glycerol to BTX aromatics has been investigated over HZSM-5 and Zn-promoted HZSM-5 catalysts. The reaction pathway of glycerol to aromatics was proposed. Glycerol was first dehydrated to three main intermediates, propenal, acetaldehyde, and acetol. The combination of oxygenate pool and olefin oligomer formed heavy aromatics in the hydrocarbon pool via oligomerization and cyclization. The disproportion and cracking of the hydrocarbon pool generated aromatics and also short alkanes. The effects of zeolite acid properties to the aromatization of glycerol were investigated over HZSM-5 with various SiO_2/Al_2O_3 ratios i.e. 23, 30, 50, 80, and 280. In order to improve the aromatics selectivity, the dehydrogenation metal, Zn was promoted on the HZSM-5 zeolites by both aqueous phase ion-exchange (IE) and incipient wetness impregnation (IWI) methods. XPS, EXAFS, H_2-TPR, and TPD-IPA (temperature programmed desorption of isopropylamine) were employed to investigate the active species of Zn in aromatization of glycerol. By using aqueous phase ion-exchange method, the appearance of Zn species was only in the form of bivalent Zn cations at exchanged site. Due to the exchange of these species with strong Brønsted acid site, the formation of aromatics tended to increase by suppressing the hydrogen transfer reaction and formation of light paraffins. ZnO species, formed by incipient wetness impregnation method was found to be less active for the reaction.

Keywords: glycerol, aromatic, zinc species, HZSM-5

4.2 Introduction

Aromatics are in widespread used as feedstocks for numerous chemical industrial processes. The conventional processes, catalytic reforming of heavy naphtha and aromatization of light paraffins are the traditional routes for these aromatics production [1]. However, both processes relied on the nonrenewable resources of crude petroleum oil and coal. Due to the shortage of petroleum resources and the rising environmental concern, the use of renewable resources has gained more attention. As one of the biomass-derived oxygenated hydrocarbons, glycerol is obtained approximately 10 wt % as by-product during the biodiesel production via transesterification reaction of vegetable oils and animal fats [2-4]. The worldwide growth of biodiesel production is leading to a continued increase in the glycerol supply and also decrease in the glycerol price. For these reasons, recent studies have investigated ways to convert glycerol to more valuable chemicals such as 1-hydroxyacetone [5], formaldehyde [6], fuel additives [7], acrolein [8-10], acetol [6], and alkyl aromatics [11]. Several studies have investigated the reaction pathway for transformation of glycerol to olefins [12, 13]. However, from the best of our knowledge, no literature dedicated to classify the details of intermediates evolution to aromatics has been published.

Herein, we report the one-step transformation of glycerol to aromatics over various SiO_2/Al_2O_3 ratios of HZSM-5 catalysts. Due to its shape selectivity and suitable acid properties, HZSM-5 showed the superior catalytic performance in converting glycerol to aromatics [11, 14, 15]. To enhance the activity and selectivity to BTX aromatics, dehydrogenation promoter, Zn, is incorporated to the HZSM-5 zeolites [16]. Broadly speaking, HZSM-5 zeolites modified with Zn are active catalysts for the aromatization of light alkanes [17-20]. The modified Zn promotes the formation of aromatics by decrease the strong Brønsted acid sites, suppressed the paraffins formation and play a key role in the dehydrogenation reaction for the formation of olefins [16] whereas the Brønsted acid sites of HZSM-5 are responsible for oligomerization and aromatization of the resulting olefins [21]. Although addition of Zn has been found very effective, the Zn species that enhanced aromatization reaction is still a matter of dispute.

The methods of Zn introduction had a strong influence to the formation of different Zn species [22]. By using the conventional incipient wetness impregnation (IWI) and ion exchange (IE) techniques, Zn/HZSM-5 was found to contain (i) isolated Zn^{2+} ions exchanged at the cation-exchange site of the zeolite, (ii) ZnO species [21, 22] and (iii) $[ZnOZn]^{2+}$ resulting from the condensation of partially hydrolyzed $ZnOH^{+}$ [20, 23]. Aleksandrov and co-workers used the linear combination of Gaussian-type orbitals fitting-functions density functional method (LCGTO-FF-DF) to study the structure and stability of different Zn species, Zn^{2+}, $ZnOH^{+}$, $Zn(H_2O)^{2+}$, and $ZnOZn^{2+}$ [24]. They concluded that the formation of $[ZnOZn]^{2+}$ from $ZnOH^{+}$ or $Zn(H_2O)^{2+}$ was energetically unfavorable which was accepted very well with the previous studies [25-27]. The activity of isolated Zn^{2+} ions at exchanged site of the zeolite and ZnO species was studied by Yu *et al.* [16, 28]. They used pyridine-IR and UV-vis absorption spectra confirmed the generation of Zn cations at exchanged site and ZnO cluster. The Zn cations at exchanged site promoted the aromatization reaction by suppressing the multiple oligomerization cracking steps for C_3 formation and facilitating the dehydrogenation reactions for the formation of aromatics, where as the formation of large ZnO particle resulted in the decreasing of aromatics yield by blocking the pore of HZSM-5. However, from the theoretical calculations, the C-H activation by extra-framework O ligands of oxygenated Zn complexes is more favorable than the lattice oxygens of the zeolite due to its higher basicity and affinity towards H^{+} [29]. The crucial role of ZnO species on HZSM-5 for alkane activation has been demonstrated by Stepanov *et al.* [30-35].

In order to investigate the effect of each Zn species to the aromatization activity, we varied the amount of Zn loadings and the loading techniques, which are IE and IWI methods. The comparable amount of Zn prepared by both methods was confirmed by atomic absorption spectroscopy (AAS). The species of Zn was studied by X-ray photoelectron spectroscopy (XPS) and extended X-ray absorption fine structure (EXAFS).

4.3 Experimental

4.3.1 Catalyst Preparation

The NH_4ZSM-5 zeolites with SiO_2/Al_2O_3 ratios of 23, 30, 50, 80, and 280 were provided by Zeolyst International. The powdered catalysts were pelletized and sieved to 20 – 40 mesh to attain the suitable catalyst packing in the reactor. The catalysts were calcined in air at 550 °C with a heating rate of 10 °C/min for 5 h. The obtained catalysts are denoted as HZSM-5 (x), where x is the SiO_2/Al_2O_3 ratios of HZSM-5. In order to study the effects of different Zn species, Zn-promoted HZSM-5 catalysts were prepared by IE and IWI methods.

*y*Zn/HZSM-5 (IWI) catalysts were prepared by incipient wetness impregnation of HZSM-5 (30), where y refers to the Zn loading (wt %). The HZSM-5 (4 g) was impregnated with the aqueous solution containing desired amount of $Zn(NO_3)_2.H_2O$, followed by dried in an oven at 120 °C overnight and calcined at 550 °C (heating rate of 10 °C/min) in air for 5 h.

*y*Zn/HZSM-5 (IE) catalysts were prepared by aqueous phase ion-exchange method. The HZSM-5 (30) was stirred in an aqueous solution of 0.005 – 0.05 M $Zn(NO_3)_2.H_2O$ at 70 °C for 12 h. Subsequently, the obtained catalysts were washed with excess distilled water, followed by dried in an oven at 120 °C overnight and calcined at 550 °C (heating rate of 10 °C/min) in air for 5 h.

4.3.2 Characterization

The relative crystallinities of the HZSM-5 zeolites before and after loading Zn was analyzed by a Rigaku X-ray diffractometer (XRD) with Cu tube for generating CuKα radiation (λ = 1.5418 Å) at room temperature. The 2θ is in the range between 5 and 40 with a scanning rate of 5 °/min. Zn loadings on the catalysts were determined by atomic absorption spectroscopy (AAS). The specific surface area and micropore volume of the samples were measured by the Brunauer-Emmet-Teller (BET) method. The temperature-programmed reduction (TPR) of Zn/HZSM-5 was performed under a reducing gas containing 10% H_2 in Ar with a thermal conductivity detector. The temperature was raised from 30-800 °C with a heating rate of 10 °C/min. The temperature programmed desorption of isopropylamine (IPA-TPD), water (H_2O-TPD), and ammonia (NH_3-TPD) were performed in a homemade flow

apparatus using a quarter inch quartz tube reactor connected to an online MS detector (MKS Cirrus). The IPA-TPD and H_2O-TPD experiments were carried out in the range of 30-800 °C at a ramp rate of 20 °C/min, whereas NH_3-TPD experiment was monitored at the range of 150-700 °C at a heating rate of 10 °C/min. The X-ray photoelectron spectroscopy (XPS) of Zn/HZSM-5 samples was conducted using a Kratos Ultra X-ray photoelectron spectrometer. The monochromatic AlKα was used as an X-ray source (anode HT = 15 kV). The XPS peaks were referenced to the binding energy of C (1s) peak at 285 eV. The local properties of Zn atom was analyzed by an extended X-ray absorption fine structure (EXAFS) technique, performed at beamline BL8 station, Synchrotron Light Research Institute (SLRI), operated at 2.5 GeV with 10^6-10^8 mA of ring current. The data were recorded in fluorescence mode at room temperature using Ge(220) double crystal monochromator. The data analysis was performed using Arthena version 0.9.18.2.

4.3.3 Catalytic Activity Testing

The pure glycerol (>99.99%) was fed together with a N_2 carrier at a flowrate giving a molar ratio of N_2/glycerol of 10:1. The reaction was carried out at temperature of 400 °C, pressure of 300 psig, and W/F ranged from 0.07 to 1 h. The liquid products, including water, were collected in a cold trap and analyzed by an Agilent 5890 gas chromatograph equipped with a capillary HP-INNOWAX column. Non-condensed products were analyzed on-line by a Shimadzu GC-17A gas chromatograph equipped with a capillary HP-PLOT/Al_2O_3 "S" deactivated column.

4.4 Results and Discussion

4.4.1 Reaction Pathway for Converting Glycerol to Aromatics

In order to study the reaction pathway of converting glycerol to aromatics, the product selectivity as a function of W/F was plotted as shown in Fig. 4.1. The product mixture consisted of propenal, acetol, acetaldehyde, olefins (ethylene and propylene), paraffins (C_1-C_3), aromatics (mainly C_6-C_9), alcohol and ketone (methanol, propen-2-ol and acetone), acid (acetic and propionic) and propanal. At the lowest contact time (W/F of 0.07 h), the major products were propenal, acetol, and acetaldehyde, indicating that the first step of glycerol

conversion was dehydration involving the central –OH and terminal –OH of glycerol resulted in two intermediate enols, which were tautomerized to 3-hydroxypropionaldehyde and acetol, respectively [8]. Since 3-hydroxypropionaldehyde was unstable, it was readily dehydrated to the more stable aldehyde as propenal while acetaldehyde and formaldehyde would be produced as a decomposed products though retro-aldol condensation [8]. Formaldehyde might further hydrogenation to methanol [36]. Light paraffins mainly methane and ethane also occurred by cleavage of C-C bonds of the unsaturated glycol, formed dehydration of glycerol over the acid sties of HZSM-5 [37].

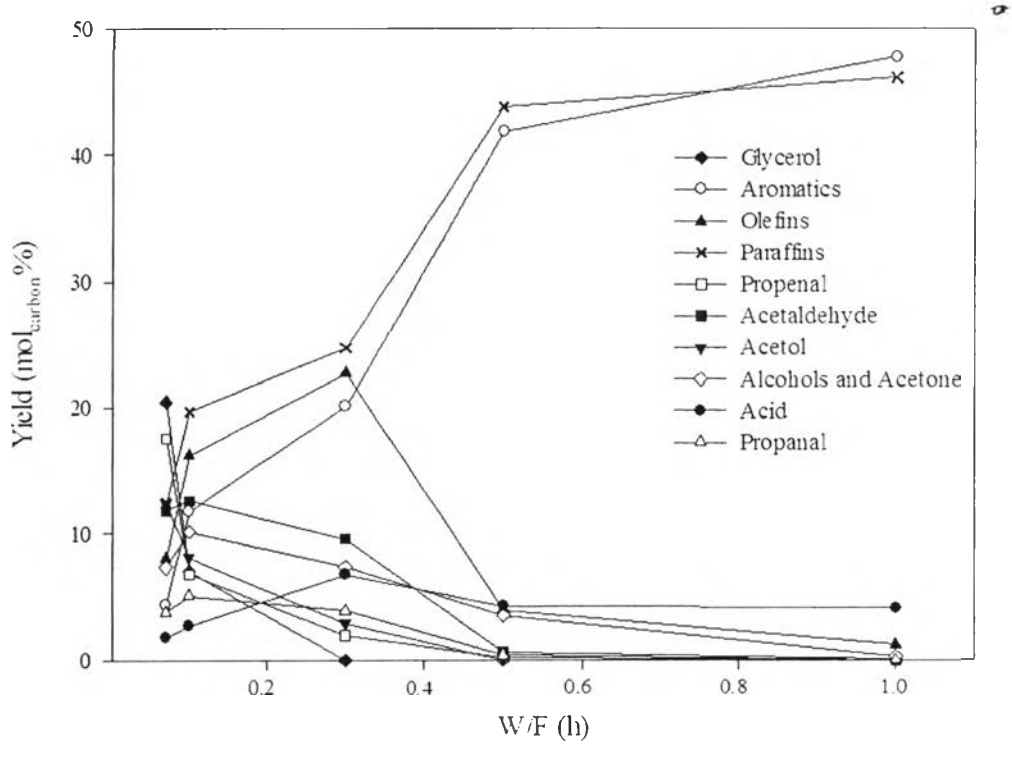

Figure 4.1 Product yield of glycerol conversion over HZSM-5 with SiO_2/Al_2O_3 ratio of 80 as a function of space time (W/F). Reaction conditions: 300 psig, 400 °C, and TOS = 3 h.

As W/F increased, the propenal decreased which corresponded to the increase of propen-2-ol and propanal. This could be implied that the hydrogenation of propenal could occur by using H-transfer, coke, and olefins as a H-doner species [8].

It has been proposed that propanal (produced via selective hydrogenation of C=C of propenal) is readily converted to aromatic hydrocarbons via acid-catalyzed aldol condensation, cyclization and dehydration [11]. The aldol condensation of resulted aldehyde generated acetaldol, further dehydrated to crotonaldehyde. The Meerwein-Ponndorf-Verley reaction between crotonaldehyde and ethanol obtained acetaldehyde and crotyl alcohol, dehydrated to butadiene [12]. From the experiment, the production of butane was almost negligible and this can be explained by the cracking of butylenes to form ethylene. Methanol which might come from unstable formaldehyde, could be further converted to aromatic hydrocarbons via oligomerization [15].

The evolution of olefin oligomers and oxygenate pool (propenal, propanal, propen-2-ol and methanol) with W/F indicated that these are intermediates for aromatic formation. The results show that these compounds tended to react themselves or each other to produce aromatics via oligomerization and dehydration. The higher light paraffins also produced from alkylation, disproportionation and cracking reactions from a surface of hydrocarbon pool (heavy aromatics) to form BTX aromatics [11]. Acetone and propionic acid might be generated from hydrogenation and isomerization of acetol. From the results, acetone might be further converted to acetic acid via oxygenation reaction or to olefins via deoxygenation because acetone was not found at the higher W/F. From the analysis of the product distribution of glycerol over HZSM-5 as a function of W/F, the reaction pathway was proposed, as summarized in Fig. 4.2.

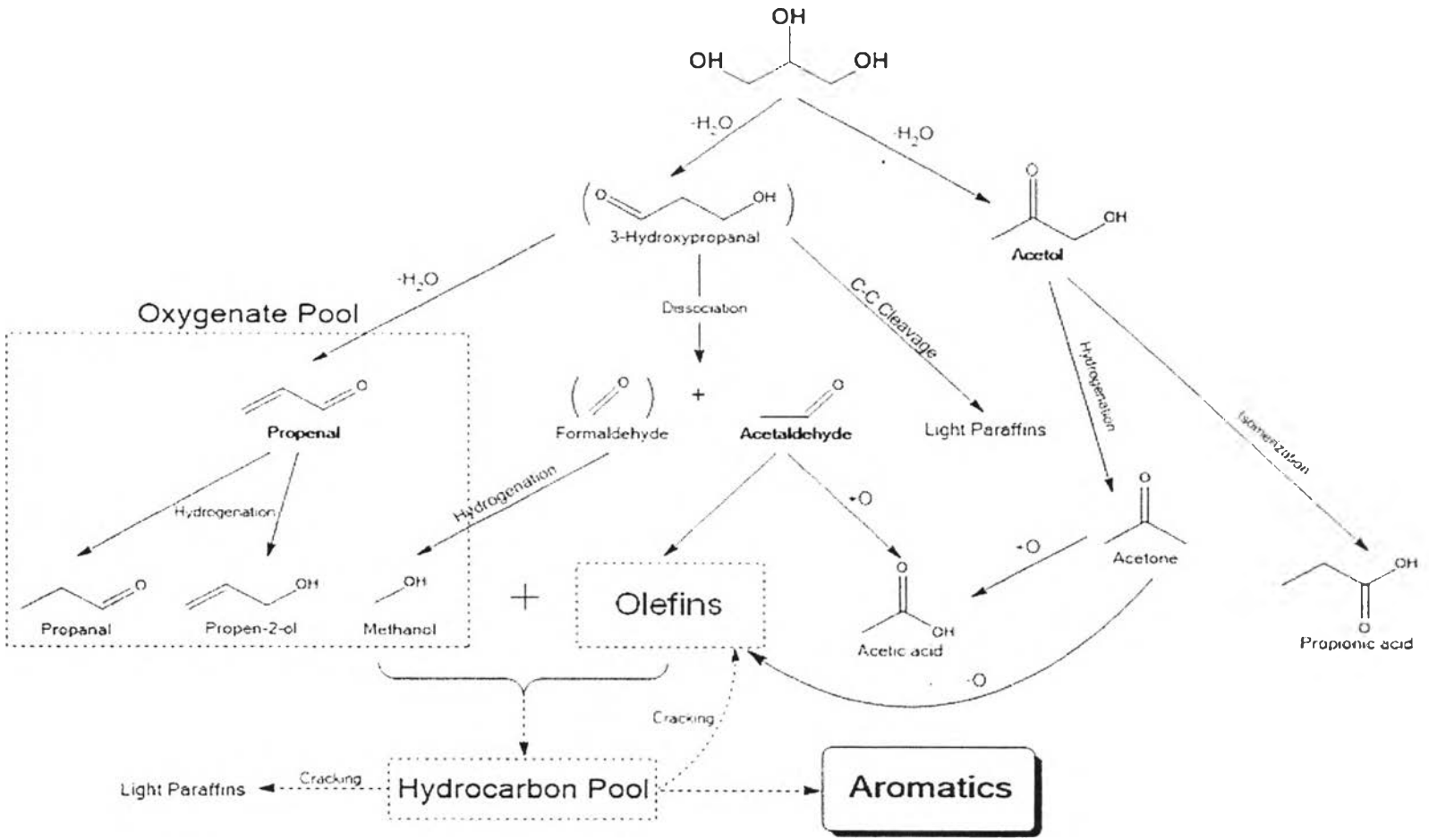

Figure 4.2 Proposed reaction pathway for converting glycerol to aromatics.

4.4.2 Effect of SiO_2/Al_2O_3 Ratios

To investigate the effect of acid properties, various SiO_2/Al_2O_3 ratios, including 23, 30, 50, 80, and 280, were tested in the conversion of glycerol to aromatic at 400 °C and 300 psig. Fig. 4.3 shows the glycerol conversion and product yields obtained over HZSM-5 with different SiO_2/Al_2O_3 ratios.

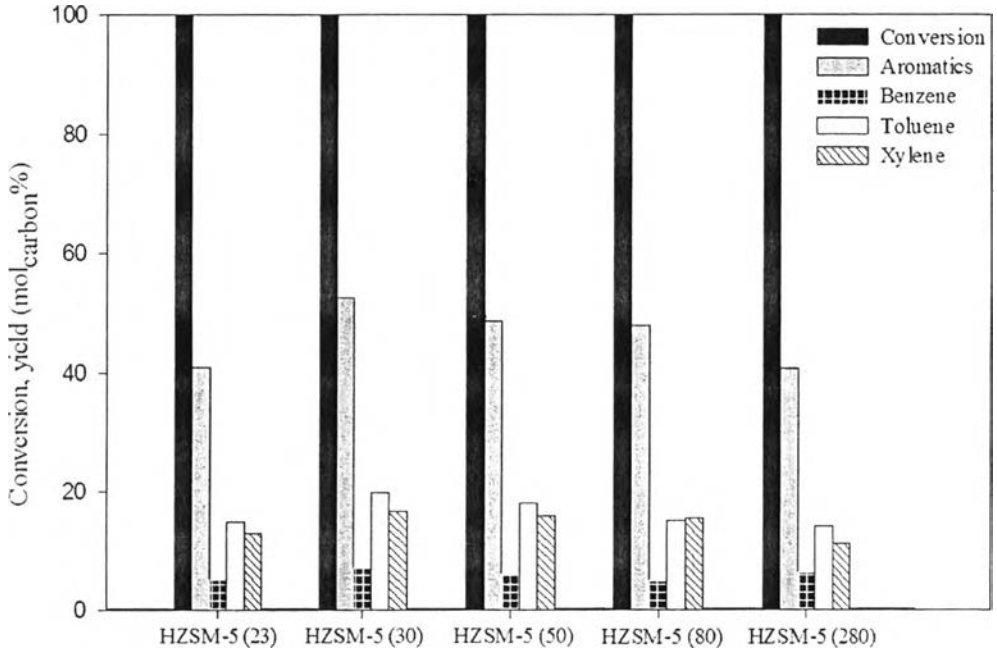

Figure 4.3 Effect of SiO_2/Al_2O_3 ratios of HZSM-5 zeolite on the glycerol conversion and aromatics yield. Reaction conditions: 300 psig, 400 °C, WHSV = 1 h^{-1}, and TOS = 3 h.

All the zeolites exhibited a complete glycerol conversion with different aromatics yields. The aromatics yield tended to decrease in the following order: HZSM-5(30) > HZSM-5(50) > HZSM-5(80) > HZSM-5(23) > HZSM-5(280). It is well known that the decrease of SiO_2/Al_2O_3 ratios results in the increase of acidity, facilitating the aromatization reaction. However, the strong Brønsted acid site also enhanced the formation of coke. The temperature programmed oxidation of spent catalysts was used to investigate amount and nature of coke, shown in Fig. 4.3. The results indicated that even the amounts of coke were different, most of the spent

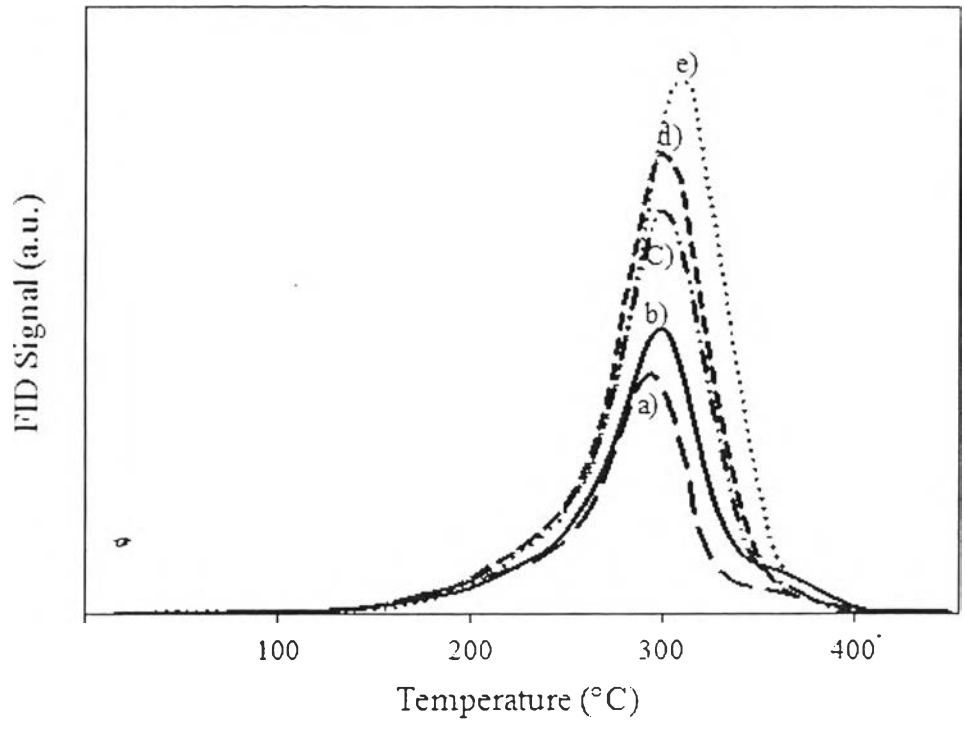

Figure 4.4 TPO profiles of spent HZSM-5 with SiO_2/Al_2O_3 ratios of a) 280, b) 23, c) 80, d) 50, and e) 30.

catalysts showed the same nature of coke, detected at temperature around 250 – 350 °C. Except in the case of spent HZSM–5 (23) catalyst, not only the peak at 250 – 350 °C but the the results also confirmed the existing of hard coke at 350 – 400 °C. It is reasonable to explain that the lower catalytic activity of HZSM–5 (23) might be resulted from the formation of hard coke, deposited in the HZSM–5 pore, lower the catalytic active site. Although HZSM-5(30) showed the highest performance in aromatization of glycerol, with aromatics yield of 52.42 mol_{carbon}% (BTX 39.66 mol_{carbon}%), a large amount of paraffins were also generated during the reaction.

4.4.3 Effect of Zn and Preparation Techniques

In order to improve the aromatics yield, Zn promoter, which is typically used in aromatization of alcohol, was incorporated in HZSM-5(30) zeolites. To avoid the negative effect of Zn loading to the textural properties of HZSM-5 zeolites, the amount of Zn loading was controlled to not more than 1 wt %. Table 4.1

shows the amount of Zn-containing HZSM-5 zeolites prepared by both IE and IWI methods.

Table 4.1 Analysis of Zn loadings, textural properties, and acidity of HZSM-5 and Zn/HZSM-5 catalysts prepared by aqueous phase ion-exchange (IE) and incipient wetness impregnation (IWI) methods

Catalysts	Zn loading (wt %)	S_{BET} (m^2/g_{cat})	Acidity [a] ($\mu mol/g_{cat}$)
HZSM-5 (23)	0	348.0	599
HZSM-5 (30)	0	389.9	373
HZSM-5 (50)	0	356.3	335
HZSM-5 (80)	0	340.8	258
HZSM-5 (280)	0	381.3	88
0.45Zn/HZSM-5 (IE)	0.45	375.7	290
0.48Zn/HZSM-5 (IE)	0.48	356.0	287
0.59Zn/HZSM-5 (IE)	0.59	346.9	255
0.64Zn/HZSM-5 (IE)	0.64	345.5	192
0.88Zn/HZSM-5 (IWI)	0.88	338.8	237

[a] The acidity was determined from IPA-TPD. The mass monitored was propylene ($m/e = 41$).

It is worth to note that the Zn loadings were less than the theoretical exchange capacity of 3.0 wt % for HZSM-5 (30) zeolite [16]. The BET results showed the comparable surface area and micropore volume because of the small amount and highly dispersed Zn over HZSM-5 zeolites (Table 1). The XRD results illustrated the same intensity of all samples, which can be assumed that the structure of HZSM-5 zeolites remained intact after Zn loading (Fig. 4.5).

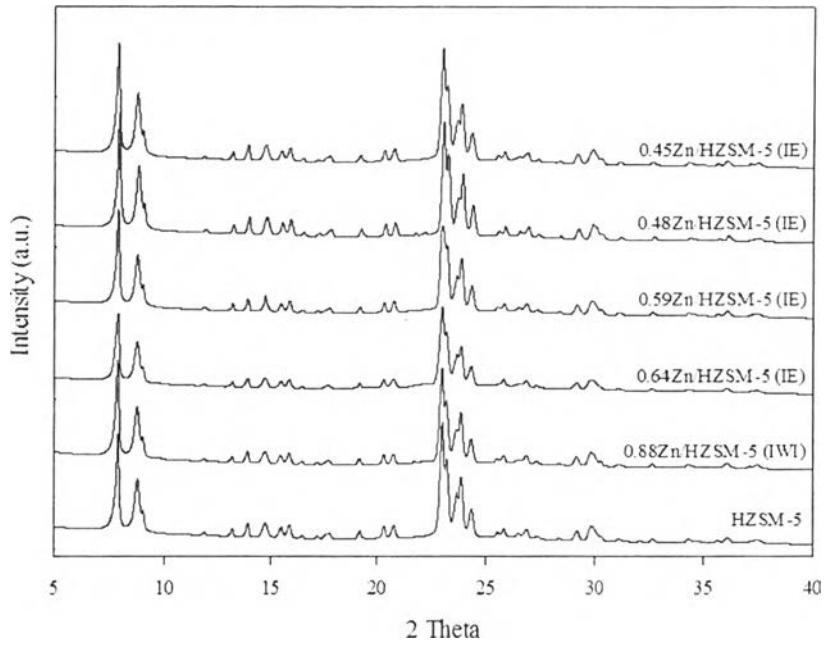

Figure 4.5 XRD patterns of HZSM-5 and Zn/HZSM-5 zeolites prepared by aqueous phase ion-exchange (IE) and incipient wetness impregnation (IWI) methods.

For *y*Zn/HZSM-5 (IE), Fig. 4.6 shows the TPD profiles of adsorbed isopropylamine, used to quantify the remaining of Brønsted acid sites, as it is a technique which allows us to monitor the desorbed ammonia and propylene from the decomposition of isopropylamine over Brønsted acid (Hofmann elimination reaction) [38]. The quantification of the strong Brønsted acid sites was measured by the amount of propylene desorbed at 350 °C. As compared with the parent HZSM-5 zeolite, the significant decrease of the strong Brønsted acid sites after introducing Zn was observed. The Brønsted acid sites decreased from 373 μmol/g for HZSM-5 to 290 μmol/g for 0.45Zn/HZSM-5 (IE). Moreover after increasing Zn loading, the Brønsted acid sites tended to decreased accordingly, indicating that the incorporation of bivalent Zn cations preferentially exchanged with protons of strong Brønsted acid

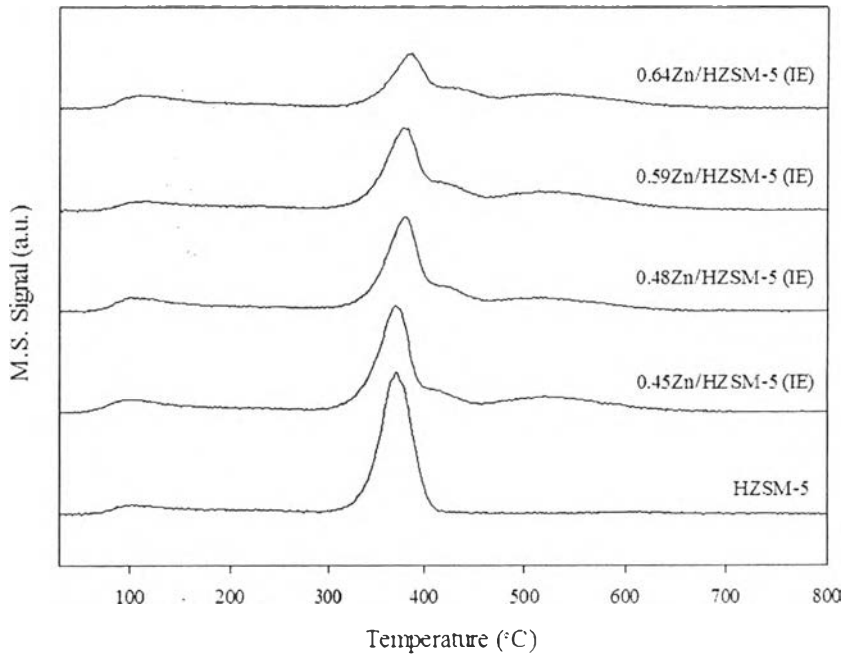

Figure 4.6 Isopropylamine-TPD (IPA-TPD) profiles of parent HZSM-5 and Zn/HZSM-5 (IE). The mass monitored was propylene (*m/e* = 41).

sites of HZSM-5 [16, 39]. From the previous research, at low SiO_2/Al_2O_3 of HZSM-5, it is almost impossible that the bivalent Zn cations will exchange with hydrogens at two adjacent framework oxygens. Therefore, the bivalent Zn cations is stabilized only on one $(AlO)^-$ center in the form of $(ZnOH)^+$ species. Fig. 4.7 represents the comparison of different Zn loading methods to the Brønsted acidity. It can be seen that the remaining Bronsted acid sites of 0.88Zn/HZSM-5 (IWI) was 237 μmol/g, which is higher than 0.64Zn/HZSM-5 (IE) (192 μmol/g). It may be concluded that with IWI method, a portion of bivalent Zn cations did not exchange with the proton of Brønsted acid site. The acid properties of *y*Zn/HZSM-5 (IE) catalysts were also determined by NH_3-TPD (Fig. 4.8).

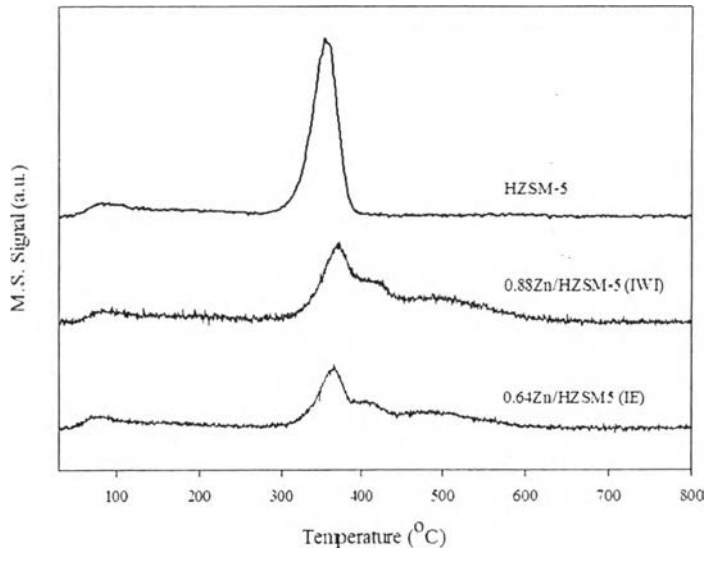

Figure 4.7 .Isopropylamine-TPD (IPA-TPD) profiles of Zn/HZSM-5 prepared by incipient wetness impregnation (0.88Zn/HZSM-5 (IWI)) and aqueous phase ion-exchange methods (0.64Zn/HZSM-5 (IE)). The mass monitored was propylene (*m/e* = 41).

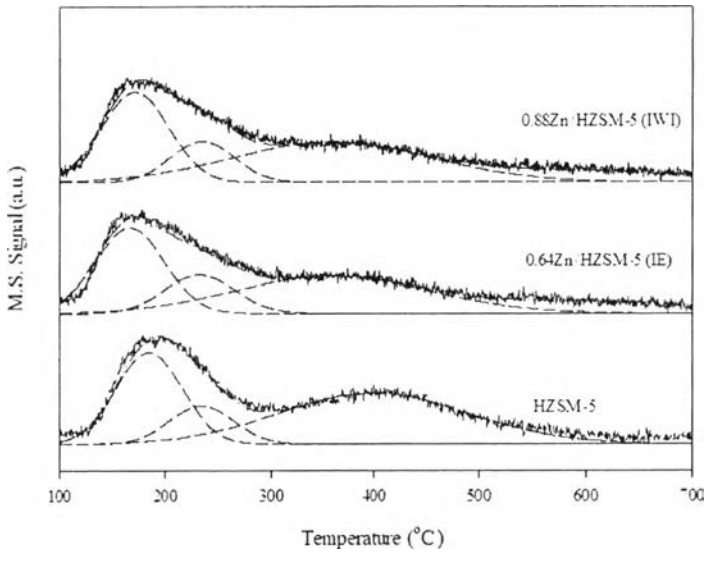

Figure 4.8 Ammonia-TPD (NH_3-TPD) profiles of Zn/HZSM-5 prepared by incipient wetness impregnation (0.88Zn/HZSM-5 (IWI)) and aqueous phase ion-exchange methods (0.64Zn/HZSM-5 (IE)). The mass monitored was ammonia (*m/e* = 17).

The species of Zn on HZSM-5 zeolite has been investigated by several research groups. It was proposed that the bivalent Zn cations could present as Zn^{2+} cations at exchanged site which replaced two Brønsted acid site, $(ZnOH)^+$, ZnO species, or binuclear $(ZnOZn)^{2+}$ clusters, formed by the partially hydrolyzed $(ZnOH)^+$ groups [20, 25, 40]. X-ray photoelectron spectroscopy (XPS) of Zn/HZSM-5 zeolites compared with pure ZnO is illustrated in Fig. 4.9. The results strongly confirmed the depending of Zn species on Zn loading method. By fitting the XPS spectra, 0.88Zn/HZSM-5 (IWI) showed 2 types of Zn species with the intensity at 1023.0 eV and 1022.0 eV while 0.64Zn/HZSM-5 (IE) showed only one peak at 1023.2 eV. It is reasonable to dedicate the higher binding energy (1023.0 eV for 0.88Zn/HZSM-5 (IWI) and 1023.2 eV for 0.64Zn/HZSM-5 (IE)) as $Zn(2p_{3/2})$ binding energy for $(ZnOH)^+$ species stabilized only on one Al center, as lattice oxygens of the zeolite have a higher electronegativity than O^{2-} group [28, 29, 39]. The presence of ZnO on 0.88Zn/HZSM-5 (IWI) can be implied by the presence of peak at 1022.0 eV. Compared with ZnO reference, the shift to higher binding energy is due to the effect of HZSM-5 framework [28]. XPS results proved that in the case of 0.88Zn/HZSM-5 (IWI), even it had a greater amount of Zn loading, but part of Zn appeared as ZnO species while the appearance of Zn species over 0.64Zn/HZSM-5 (IE) only in the form of $(ZnOH)^+$ species. The XPS results clearly explained the reason why IPA-TPD of 0.88Zn/HZSM-5 (IWI) gave a higher amount of remaining Brønsted acid sites than 0.64Zn/HZSM-5 (IE). In the case of binuclear $(Zn\text{-}O\text{-}Zn)^{2+}$ clusters, the formation of these species by conventional loading Zn method is still a controversial topic. Aleksandrov and co-workers found that the formation of $(Zn\text{-}O\text{-}Zn)^{2+}$ is energetically unfavorable, supported by the previous studies [24-27]. We confirmed the absence of $(Zn\text{-}O\text{-}Zn)^{2+}$ clusters by using EXAFS and TPR methods. EXAFS is one of the most powerful methods, used to investigate the oxidation state and local environment of Zn species over HZSM-5 zeolites. The Fourier transform of Zn K-edge for 0.64Zn/HZSM-5 (IE), 0.88Zn/HZSM-5 (IWI), ZnO powder, and Zn foil are illustrated in Fig. 4.10. The theoretical distance between nuclei Zn atom and its oxygen neighbors of ZnO reference is 1.97 Å but the results showed the shorter distance about 1.6 Å due to the radial distance measured by EXAFS is the distance between electron clouds of Zn and its oxygen neighbor atoms [20, 28].

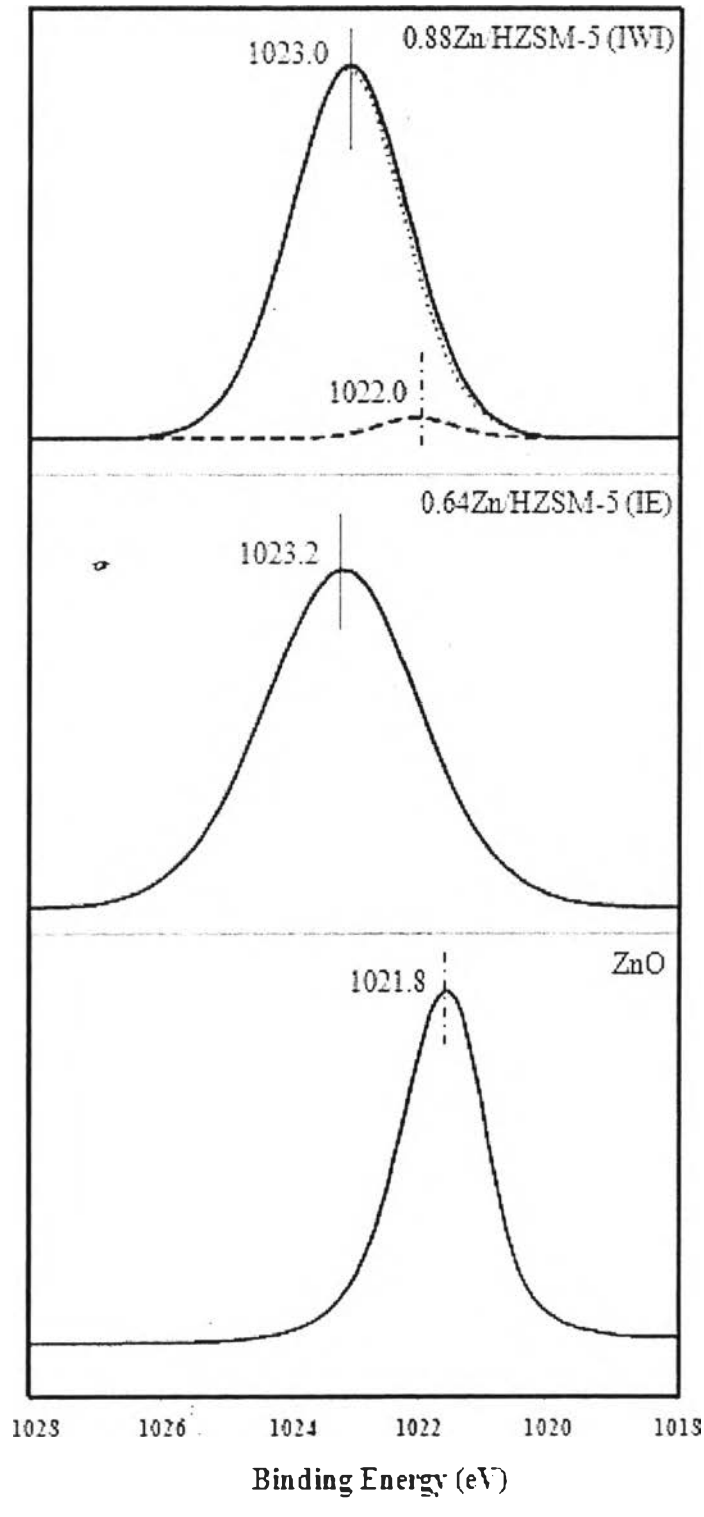

Figure 4.9 XPS spectra of Zn ($2p_{3/2}$) of 0.88Zn/HZSM-5 (IWI), 0.64Zn/HZSM-5 (IE), and ZnO.

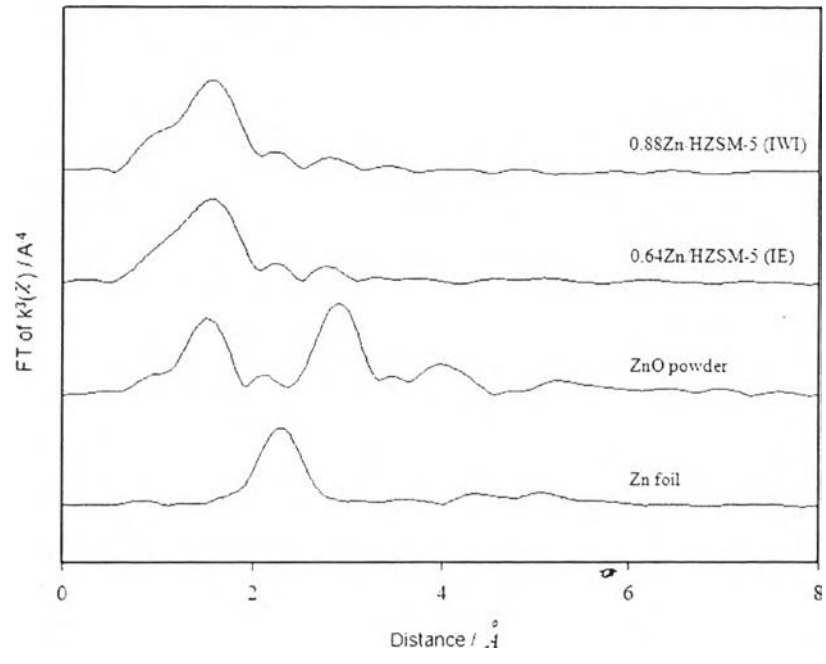

Figure 4.10 EXAFS of Zn K-edge radial distributions of 0.64Zn/HZSM-5 (IE), 0.88Zn/HZSM-5 (IWI), ZnO powder, and metallic Zn foil.

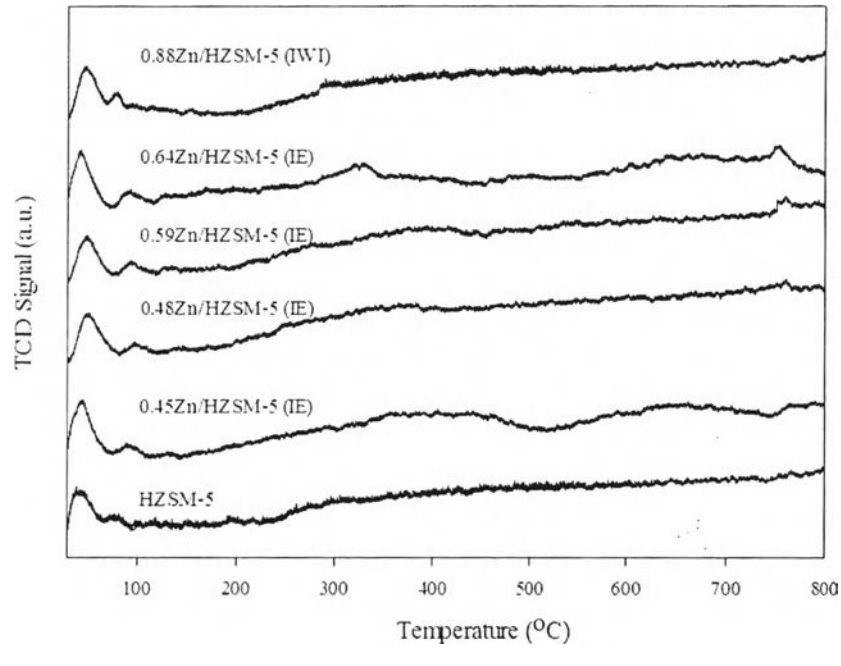

Figure 4.11 Temperature programmed reduction (TPR) profiles of 0.88Zn/HZSM-5 (IWI), 0.64Zn/HZSM-5 (IE), 0.59Zn/HZSM-5 (IE), 0.48Zn/HZSM-5 (IE), 0.45Zn/HZSM-5 (IE), and HZSM-5.

Compared with the ZnO powder, the Zn-O first shell of Zn/HZSM-5 prepared by both methods showed the higher radial distance. This results were consistent with previous report by X. Niu and co-workers [28], who suggested the shifting to higher radial distance when the formation of $(ZnOH)^+$ species existed. The Zn-Zn second shell is shown at a longer distance around 2.95 Å while the actual distance is 3.2 Å [28]. From previous mention, the XPS results indicated the formation of ZnO species over 0.88Zn/HZSM-5 (IWI) but EXAFS spectra did not show the presence of Zn-Zn contacts. From BET, XPS, and EXAFS results of 0.88Zn/HZSM-5 (IWI), it is shapely to conclude that the morphology of ZnO is highly dispersed over HZSM-5 zeolite. In addition, even the EXAFS spectra of Zn/HZSM-5 did not show the second shell of Zn-Zn, further evidence to confirm the absence of $(Zn\text{-}O\text{-}Zn)^{2+}$ cluster is needed.

The further investigation on the formation of binuclear $(Zn\text{-}O\text{-}Zn)^{2+}$ clusters was performed by H_2-TPR studies (Fig. 4.11) of Zn/HZSM-5 prepared by both IWI and IE methods. In the case of binuclear $(Zn\text{-}O\text{-}Zn)^{2+}$ clusters, El-M. and co-workers reported that the reduction peak of binuclear $(Zn\text{-}O\text{-}Zn)^{2+}$ should be found similar with the bridge Fe^{3+} complexes at temperature around 400 °C [41]. It could be seen from TPR results that all samples showed only one peak below 100 °C, which is the characteristic peak of adsorbed hydrogen on HZSM-5 zeolites [42]. These results also indicated the absence of the binuclear $(Zn\text{-}O\text{-}Zn)^{2+}$ clusters over Zn/HZSM-5, prepared by both methods.

On the whole, the species of Zn strongly depend on the preparation methods. For IE method, bivalent Zn cations exchanged with the proton at strong Brønsted acid site to form $(ZnOH)^+$ species. While, IWI method, Zn cations could form both $(ZnOH)^+$ species and ZnO species. The appearance of ZnO species is the reason why, with the comparable amount of Zn loading, the remaining of strong Brønsted acid sites in IWI method is more than IE method.

4.4.4 Effect of Zn Species in Converting Glycerol to Aromatics

*y*Zn/HZSM-5 (IE) with different Zn loadings (0.45, 0.48, 0.59, and 0.64 wt %) were studied in the aromatization of glycerol at 400 °C and 300 psig. The conversions were always 100% for all modified catalysts. The aromatic yields are illustrated in Fig. 4.12. The increasing of Zn loading resulted in the enhancement of

aromatics formation. The highest aromatic yield of 80.3 mol_{carbon}% (mainly toluene and xylene) was achieved over the highest Zn loading 0.64Zn/HZSM-5(IE) zeolite. The appearance of Zn on HZSM-5 significantly suppressed the formation of the side product light paraffins. Fig. 4.13 shows the relationship between aromatics and light paraffins yields as a function of wt % Zn loading. Compared with the parent HZSM-5, 0.64Zn/HZSM-5 (IE) showed obviously lower side products of light paraffins (7.2 mol_{carbon}%). As Zn loading increased, the formation of paraffins tended to decreased while the formation of aromatics increased. It could be summarized that the introducing of Zn species, exchanging with Brønsted acid sites remarkably enhanced the formation of aromatics by following two reasons. First, the replacing of strong Brønsted acid with Zn suppressed the cracking to light olefins. Second, the $(ZnOH)^+$ species had a high capacity in dehydrogenation reaction, enhancing the aromatics formation [16, 28].

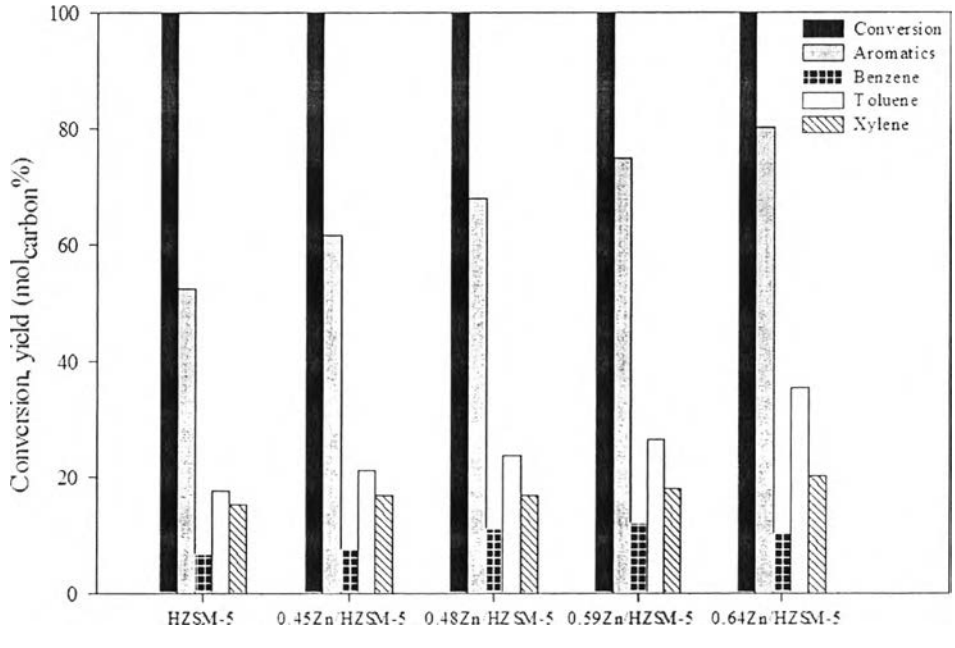

Figure 4.12 Glycerol conversion and aromatics yield as a function of Zn loading by aqueous phase ion-exchange (IE) method. Reaction conditions: 300 psig, 400 °C, WHSV = 1 h^{-1}, and TOS = 3 h.

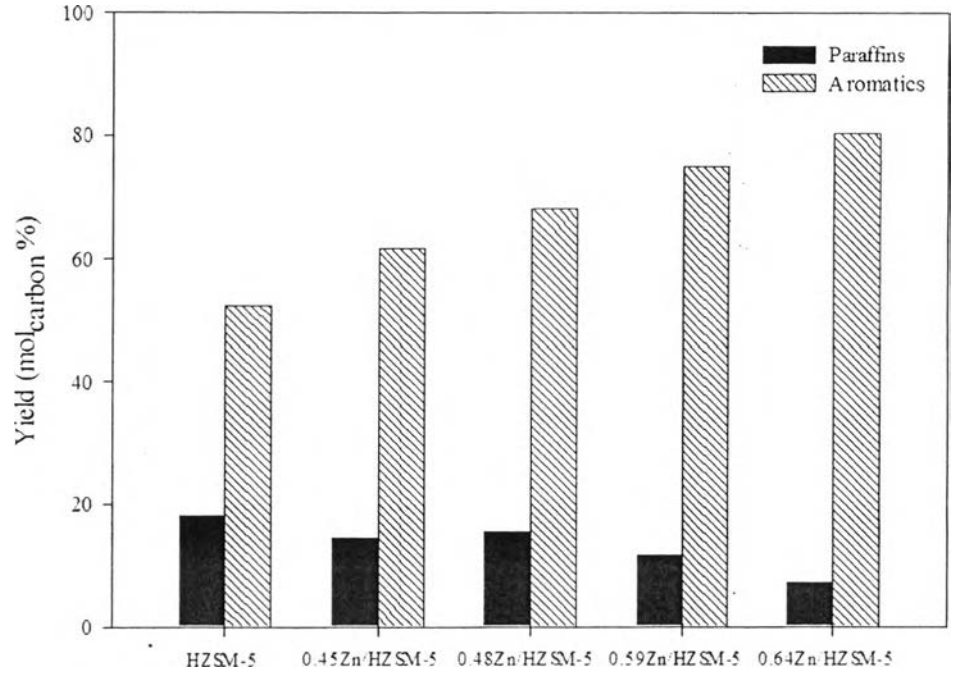

Figure 4.13 The relationship between aromatics and light paraffins yields as a function of Zn loading by aqueous phase ion-exchange (IE) method. Reaction conditions: 300 psig, 400 °C, WHSV = 1 h^{-1}, and TOS = 3 h.

In order to compare the activity of $(ZnOH)^+$ and ZnO species, the catalytic activity of 0.64Zn/HZSM-5 (IE) was compared with 0.88Zn/HZSM-5 (IWI) (Fig. 14). Under temperature of 400 °C, pressure 300 psig and WHSV equal to 3.33 h^{-1}, 0.88Zn/HZSM-5 (IWI) showed the lower aromatics yield 38.87 mol_{carbon}% compared with 43.28 mol_{carbon}% of 0.64Zn/HZSM-5 (IE). The results strongly demonstrated that the active site for aromatization of glycerol was $(ZnOH)^+$ species while the ZnO species was found to be less active for these reactions. The amount of Zn loading on the spent catalysts was also investigated by using AAS. One might proposed that the small amount of ZnO could also be formed on 0.64Zn/HZSM-5 (IE). The presence of this Zn species should be reduced and vaporized from the catalyst. However, the comparable amount of Zn loading between fresh and spent 0.64Zn/HZSM-5 (IE) catalysts also confirmed the disappear of ZnO on this Zn species on 0.64Zn/HZSM-5 (IE) catalysts.

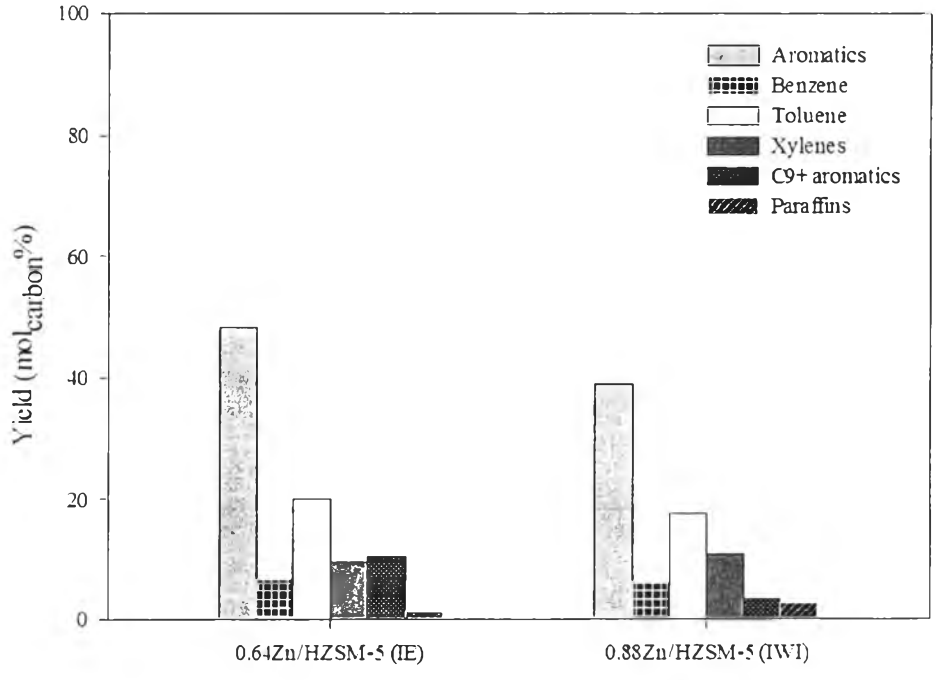

Figure 4.14 Glycerol conversion and aromatics yield as a function of preparation methods, 0.64Zn/HZSM-5 (IE) and 0.88Zn/HZSM-5 (IWI). Reaction conditions: 300 psig, 400 °C, WHSV = 3.33 h^{-1}, and TOS = 3 h.

Generally, the quantities of strong, medium, and weak acid sites over HZSM-5 zeolite were found at 300-550, 200-300, and 120-200 °C, respectively. The incorporation of Zn over HZSM-5 catalysts has a strong influence to the acid distribution. Compared with the parent HZSM-5, the increase in medium acid sites over 0.64Zn/HZSM-5 (IE) was found with the expensed of strong and weak acid sites. The generation of medium acid sites was dedicated to the interaction of Zn species and acid sites of HZSM-5 catalyst [28]. Agree well with the IPA-TPD, 0.64Zn/HZSM-5 (IE) showed the higher amount of medium acid sites than 0.88Zn/HZSM-5 (IWI), representing the higher bivalent Zn cations at exchange sites was formed (Table 4.2).

Table 4.2 Acidic properties of HZSM-5 (30) and Zn containing HZSM-5 prepared by aqueous phase ion-exchange (IE) and incipient wetness impregnation (IWI) methods

Catalysts	Acid amount (μmol NH_3/g_{cat})			
	Weak	Medium	Strong	Total
HZSM-5 (30)	235	95	378	708
0.64Zn/HZSM-5 (IE)	227	104	283	614
0.88Zn/HZSM-5 (IWI)	232	99	314	645

4.5 Conclusions

The reaction pathway for converting glycerol to aromatics has been proposed. Glycerol was first converted to propenal, acetol, and acetaldehyde. Propenal and acetol are the main intermediates of acid-catalyzed dehydration while acetaldehyde was generated by the combination of dehydration and dissociation. The carbonyl bond dissociation of acetaldehyde generated olefin products which further reacted with oxygenates (propenal, propanal, propen-2-ol and methanol), forming aromatics via oligomerization, dehydration, and cyclization. The formation of water during the reaction had a strongly impact to the catalysts properties. With the lowest SiO_2/Al_2O_3 ratio of 23, even it provided the highest acid active sites, the formation of hard coke resulted in blocking of acid active sites for aromatization reaction. HZSM-5 with SiO_2/Al_2O_3 of 30 showed the highest aromatics formation; however significant amount of light paraffins still occurred as the main side products. In order to increase the aromatics selectivity, Zn-loaded HZSM-5 zeolites were prepared by both IE and IWI methods. The $(ZnOH)^+$ species was the only species found over Zn/HZSM-5 (IE). The aromatic yield linearly increased with the increment of the bivalent Zn cations. ZnO species formed over Zn/HZSM-5 (IWI) was found to be the less active for the reaction.

4.6 Acknowledgements

The authors would like to thank Synchrotron Light Research Institute (SLRI), Thailand for providing the EXAFS measurements. The Center of Excellence on Petrochemical and Materials Technology, Chulalongkorn University, Thailand, and the Petroleum and Petrochemical College, Chulalongkorn University are also acknowledged.

4.7 References

1 D. L. Ransley, in Kirk-Orthmer Encyclopedia of Chemical Technology, third ed., Vol. 4, M.Grayson and D. Eckroth, eds., Wiley-Interscience, New york, 1978, p. 264.

2 R.S. Karinen, A.O.I. Krause, Appl. Catal. A 306 (2006) 128-133.

3 T.L. Chew, S. Bhatia, Bioresour. Technol. 99 (2008) 7911-7922.

4 G.W. Huber, A. Corma, Angew. Chem. – Int. Ed. 46 (2007) 7184–7201.

5 J.S. Vasconcelos, C.L. Lima, J.M. Filho, A.C. Oliveira, E.B. Barros, F.F. de Sousa, M.G.C. Rocha, P. Bargiela, A.C. Oliveira, Chem. Eng. J. 168 (2011) 656-664.

6 K. Pathak, K.M. Reddy, N.N. Bakhshi, A.K. Dalai, Appl. Catal. A 373 (2010) 224-238.

7 H. Serafim, I.M. Fonseca, A.M. Ramos, J. Vital, J.E. Castanheiro, Chem. Eng. J. 178 (2011) 291-296.

8 A. Corma, G.W. Huber, L. Sauvanaud, P. O'Connor, J. Catal. 257 (2008) 163–171.

9 A.S. de Oliveira, S.J.S. Vasconcelos, J.R. de Sousa, F.F. de Sousa, J.M. Filho, A.C. Oliveira, Chem. Eng. J. 168 (2011) 765-774.

10 B. Katryniok, S.Paul, M. Capron, F. Dumeignil, ChemSusChem. 2 (2009) 719-730.

11 T.Q. Hoang, X. Zhu, T. Danuthai, L.L. Lobban, D.E. Resasco, R.G. Mallinson, Energy Fuels 24 (2010) 3804-3809.

12 Z.Y. Zakaria, J. Linnekoski, N.A.S. Amin, Chem. Eng. J. 207-208 (2012) 803-813.

13 Z.Y. Zakaria, N.A.S. Amin, J. Linnekoski, Biomass and Bioenergy 55 (2013) 370-385.

14 Y.T. Kim, K.D. Jung, E.D. Park, Microporous and Mesoporous Mater. 131 (2010) 28-36.

15 Y. Ni, W.P.A. Sun, W. Mo, J. Hu, T. Li, G. Li, Journal of Industrial and Engineering Chemistry 16 (2010) 503-505.

16 L. Yu, S. Huang, S. Zhang, Z. Liu, W. Xin, S. Xie, L. Xu, ACS Catal. 2 (2012) 1203-1210.

17 Y. Ono, Catal. Rev. Sci. Eng. 34 (1992) 179.

18 A.R. Hagen, F. Roessner, Catal. Rev. Sci. Eng. 42 (2000) 403.

19 J.A. Biscardi, E. Iglesia, J. Catal. 182 (1999) 117.

20 J.A. Biscardi, G. D. Meitzner, E. Iglesia, J. Catal. 179 (1998) 192-202.

21 S.M.T. Almutairi, B. Mezari, P.C.M.M. Magusin, E.A. Pidko, E.J.M. Hensen, ACS Catal. 2 (2012) 71-83.

22 H. Berndt, G. Lietz, B. Lucke, J. Volter, Appl. Catal. A 146 (2001) 351-363.

23 J. Xu, A. Zheng, X. Wang, G. Qi, J. Su, J. Du, Z. Gan, J. Wu, W. Wang, F. Deng, Chem. Sci. 3 (2012) 2932.

24 H.A. Aleksandrov, G.N. Vayssilov, N. Rosch, J. Mol. Catal. A: Chem. 256 (2006) 146-155.

25 A.L. Yakovlev, A.A. Shubin, G.M. Zhidomirov, R.A.V. Santen, Catal. Lett. 70 (2000) 175-181.

26 A.T. Bell, G. Centi, B. Wichterlowa, A.T. Bell (Eds.), Kluwer Academic Publishers, Dordrecht (2000) 55-73.

27 M.J. Rice, A.K. Chakraborty, A.T. Bell, J. Phys. Chem. B 104 (2000) 9987-9992.

28 X. Niu, J. Gao, Q. Miao, M. Dong, G. Wang, W. Fan, Z. Qin, Microporous and Mesoporous Mater. 197 (2014) 252-261.

29 E.A. Pidko, R.A.V. Santen, J. Phys. Chem. C 111 (2007) 2643.

30 A.A. Gabrienko, S.S. Arzumanov, D. Freude, A.G. Stepanov, J. Phys. Chem. C 114 (2010) 12681.

31 S.S. Arzumanov, A.A. Gabrienko, D. Freude, A.G. Stepanov, Solid State Nucl. Magn. Reson. 35 (2009) 113.

32 A.G. Stepanov, S.S. Arzumanov, A.A. Gabrienko, V.N. Parmon, I.I. Ivanova, D. Freude, Chem. Phys. Chem. 9 (2008) 2559.

33 A.G. Stepanov, S.S. Arzumanov, V.N. Parmon, Y.G. Kolyagin, I.I. Ivanova, D. Freude, Catal. Lett. 114 (2007) 85.

34 A.G. Stepanov, S.S. Arzumanov, A.A. Gabrienko, A.V. Toktarev, V.N. Parmon, D. Freude, J. Catal. 253 (2008) 11.

35 A.A. Gabrienko, S.S. Arzumanov, A.V. Toktarev, I.G. Danilova, D. Freude, A.G. Stepanov, Phys. Chem. Chem. Phys. 12 (2010) 5149.

36 E. Tsukuda, S. Sato, R. Takahashi, T. Sodesawa, Catal. Commun. 8 (2007) 1349–1353.

37 K. Murata, I. Takahara, M. Inaba, React. Kinet. Catal. Lett. 93 (2008) 59-66.

38 T.J.G. Kofke, R.J. Gorte, G.T. Kokotailo, W.E. Farneth, J. Catal. 115 (1989) 265-272.

39 S.M.T. Almutairi, B. Mezari, P.C.M.M. Magusin, E.A. Pidko, E.J.M. Hensen. ACS Catal. 2 (2012) 71-83.

40 J.A. Biscardi, E. Iglesia, Catal. Today 31 (1996) 207-231.

41 El-M. El-Malki, R.A.V. Santen, W.M.H. Sachtler, J. Phys. Chem. B 103 (1999) 4611-4622.

42 S.Todorova, K. Tenchev, B.L. Su, Stud. Surf. Sci. Catal. 158 (2005) 1725-1732.